TYPE Original Research
PUBLISHED 03 March 2025
DOI 10.3389/fmars.2025.1556480

OPEN ACCESS

EDITED BY
Xiaojian Zhang,
Nanjing University, China

REVIEWED BY
Simin Peng,
Jiangxi Normal University, China
Fucai Duan,
Zhejiang Normal University, China

*CORRESPONDENCE
Yu-Min Chou
chouym@sustech.edu.cn
Qingsong Liu
qsliu@sustech.edu.cn

RECEIVED 07 January 2025
ACCEPTED 17 February 2025
PUBLISHED 03 March 2025

CITATION
Li H, Tang J, Zhong Y, Ning L, Liu J, Sun C, Zhang W, Chou Y-M and Liu Q (2025) External and internal forcings controlled the precipitation patterns in eastern China over the past millennium. *Front. Mar. Sci.* 12:1556480. doi: 10.3389/fmars.2025.1556480

External and internal forcings controlled the precipitation patterns in eastern China over the past millennium

Hai Li[1,2], Jianhui Tang[3], Yi Zhong[2], Liang Ning[4], Jiabo Liu[5], Chijun Sun[6], Weijie Zhang[2], Yu-Min Chou[2*] and Qingsong Liu[2*]

[1]Southern Marine Science and Engineering Guangdong Laboratory (Guangzhou), Guangzhou, China, [2]Centre for Marine Magnetism (CM[2]), Department of Ocean Science and Engineering, Southern University of Science and Technology, Shenzhen, China, [3]Key Laboratory of Coastal Environmental Processes and Ecological Remediation, Yantai Institute of Coastal Zone Research, Chinese Academy of Sciences, Yantai, China, [4]Key Laboratory for Virtual Geographic Environment, Ministry of Education, Nanjing Normal University, Nanjing, China, [5]Paleomagnetism and Planetary Magnetism Laboratory, School of Geophysics and Geomatics, China University of Geosciences, Wuhan, Hubei, China, [6]Department of Earth and Planetary Sciences, University of California, Davis, Davis, CA, United States

The Asian Summer Monsoon provides critical water source to over a billion people. However, there is mounting evidence regarding how precipitation associated with the Asian Summer Monsoon varies spatially and temporally, prompting further exploration of the underlying mechanisms. Here, we reconstruct a ~2900-year summer precipitation record through grain-size and clay analyses of core M5-8 retrieved from the Bohai Sea in China. Our records indicate that the warm (cold) phase of the Atlantic Multidecadal Variability significantly increases (decreases) summer precipitation in North China through atmosphere-ocean feedback and circum-global teleconnection. Over the past millennium, eastern China exhibited a distinctive tripole pattern of summer precipitation. During the Medieval Climate Anomaly, it exhibited a positive-negative-positive structure in North, Central, and South China, respectively. In contrast, during the Little Ice Age, the pattern flipped to a negative-positive-negative structure. These patterns were influenced by external forcings, including solar activity and volcanic eruptions, which directly influenced atmospheric circulation patterns and modulated internal climate variability. Our study provides an improved understanding of the summer precipitation variability in East Asia, and emphasizes the external and internal forcings in shaping the spatial patterns of monsoon precipitation.

KEYWORDS

Asian summer monsoon, Bohai Sea, external forcing, Atlantic multidecadal variability, tripole precipitation pattern

1 Introduction

The Asian Summer Monsoon (ASM) precipitation exhibits variability across interannual, multidecadal, and centennial time scales, exerting a significant influence on the welfare of billions of residents in East Asia. The primary driver of ASM precipitation variability varies across different time scales (Wang et al., 2001, Wang et al., 2017; Cheng et al., 2016). On the orbital scale, the ASM exhibits a notable precession cycle due to the migration of the Intertropical Convergence Zone (ITCZ) in response to variations in low-latitude solar radiation (Wang et al., 2008; Cheng et al., 2016). Over the millennial scale, ASM precipitation is known to be sensitive to changes in the Atlantic Meridional Overturning Circulation (Porter and An, 1995; Wang et al., 2001). Overall, external forcings primarily drive the ASM precipitation on both orbital and millennial scales.

On centennial and multidecadal scales, the forcing factor of ASM is less well understood. On the one hand, external forcings such as solar radiation, greenhouse gases, and volcanism can affect the land-sea temperature gradient, thereby controlling the intensity of ASM (Mann et al., 2009; Chen et al., 2020). On the other hand, various oceanic and atmospheric processes, including the Intertropical Convergence Zone (ITCZ), El Niño-Southern Oscillation (ENSO), Pacific Decadal Oscillation (PDO), and North Atlantic Oscillation (NAO) are known to significantly influence ASM precipitation (Yancheva et al., 2007; Linderholm et al., 2011; Jiang et al., 2021b). Previous studies have suggested that the Atlantic Multidecadal Variability (AMV) is also a driving force of ASM precipitation variability (Lu et al., 2006; Wang et al., 2009). However, little is known about the long-term effects of AMV on ASM (Wang et al., 2013; Zhu et al., 2021), which hinders our comprehensive understanding of the ASM behavior.

Evidence from both instrumental and paleoclimate records indicates that the ASM exhibits spatial variations in precipitation intensity (e.g., Ding et al., 2008; Jiang et al., 2021a). However, there remains debate surrounding the driving forces and spatial pattern of the ASM. In recent decades, eastern China has experienced either a dipole or tripole structure (Ding et al., 2008; He et al., 2017). The dipole structure exhibits a opposite precipitation pattern from the south to north of the Yangtze River, while the tripole structure demonstrates a pattern of "+/-/+" or "-/+/-" in North-Central-South China (Ding et al., 2008; Wang et al., 2022). These precipitation structures were believed to be influenced by Western Pacific Subtropical High (WPSH), ENSO, NAO, and ASM intensity (Ding et al., 2009; Rao et al., 2016b; He et al., 2017). Similar precipitation structures were also observed during the last deglaciation (Dai et al., 2021) and the Holocene (Rao et al., 2016a). Over the past millennium, however, two distinct precipitation patterns have been identified, i.e., a dipole structure (Chen et al., 2015b) and an alternating dipole and tripole structure (Wang et al., 2022). The former was supposed to be modulated by ENSO through the shifts and intensity of WPSH, while the latter was influenced by the interactions among monsoon intensity, PDO, and AMV phases (Chen et al., 2015b; Wang et al., 2022).

In this study, we reconstructed the ASM precipitation variations from the Bohai Sea sediment grain size in North China over the past ~2900 years. This record was compared with those from Central China and South China to understand the spatiotemporal ASM precipitation patterns in eastern China (east of approximate 105°E). We then investigated the potential mechanisms of the reconstructed precipitation variations in North China and the summer precipitation patterns in eastern China, and found that they were primarily influenced by solar radiation, volcanic activity, and AMV.

2 Regional marine hydrodynamic characteristics

The Bohai Sea, with an average depth of approximately 18 meters, is a shallow marine environment exhibiting relatively low salinity due to substantial freshwater input from rivers such as the Yellow and Haihe Rivers (Li et al., 2020). Ocean circulations of the Bohai Sea include the Yellow Sea Warm Current, Liaodong Coastal Current, and Bohai Sea Coastal Current (Figure 1). Surface circulations are driven by the direction and intensity of regional seasonal winds (Wang et al., 2010). In summer, the Yellow Sea Warm Current weakens or disappears, allowing the cold Yellow Sea Water to enter through the Bohai Strait (Figure 1B). Summer winds drive northward boundary currents in shallow coastal waters (Dou et al., 2014). In winter, the high-salinity Yellow Sea Warm Current enters the Bohai Sea, splits into two branches in the northwestern Bohai Sea, forming the anti-cyclonic Liaodong Gyre (Fang et al., 2000), and creating a counterclockwise circulation influenced by the Yellow River's diluted water (Figure 1C, Zhao et al., 1995). In addition, strong winter winds cause vertical mixing and drive southward currents. These dynamical conditions and the Yellow River's sediment load produce fine-grained mud, coarse-grained sand, and mixed deposits in the Bohai Sea (Li et al., 2010; Qiao et al., 2017).

3 Materials and methods

3.1 Materials

The sediment core M5-8 (39.09°N, 120.0°E), retrieved from the central basin of the Bohai Sea at a water depth of 22 meters, is 3.46 meters long and has a grayish-black color (Figure 1). The low salinity of the Bohai Sea results in decreased foraminifera abundance in marine sediments. Efforts to identify suitable dating materials, such as shells and charcoal, in the study cores were unsuccessful, resulting in only three ^{14}C dates obtained from benthic foraminifera in core M5-8. To constrain a more reliable age-model, we used the mass magnetic susceptibility data from cores M12-8, M5-8, and BHB15-6 to refine the age-depth model, yielding additional age tie points (Li et al., 2023). The age uncertainties for these tie points were provided by the initial age-depth model, established using ^{14}C dating and calculated with *Undatable* software (Lougheed and Obrochta, 2019). The obtained age model for core M5-8, shown in Supplementary Figure 1, spans ~2900 years.

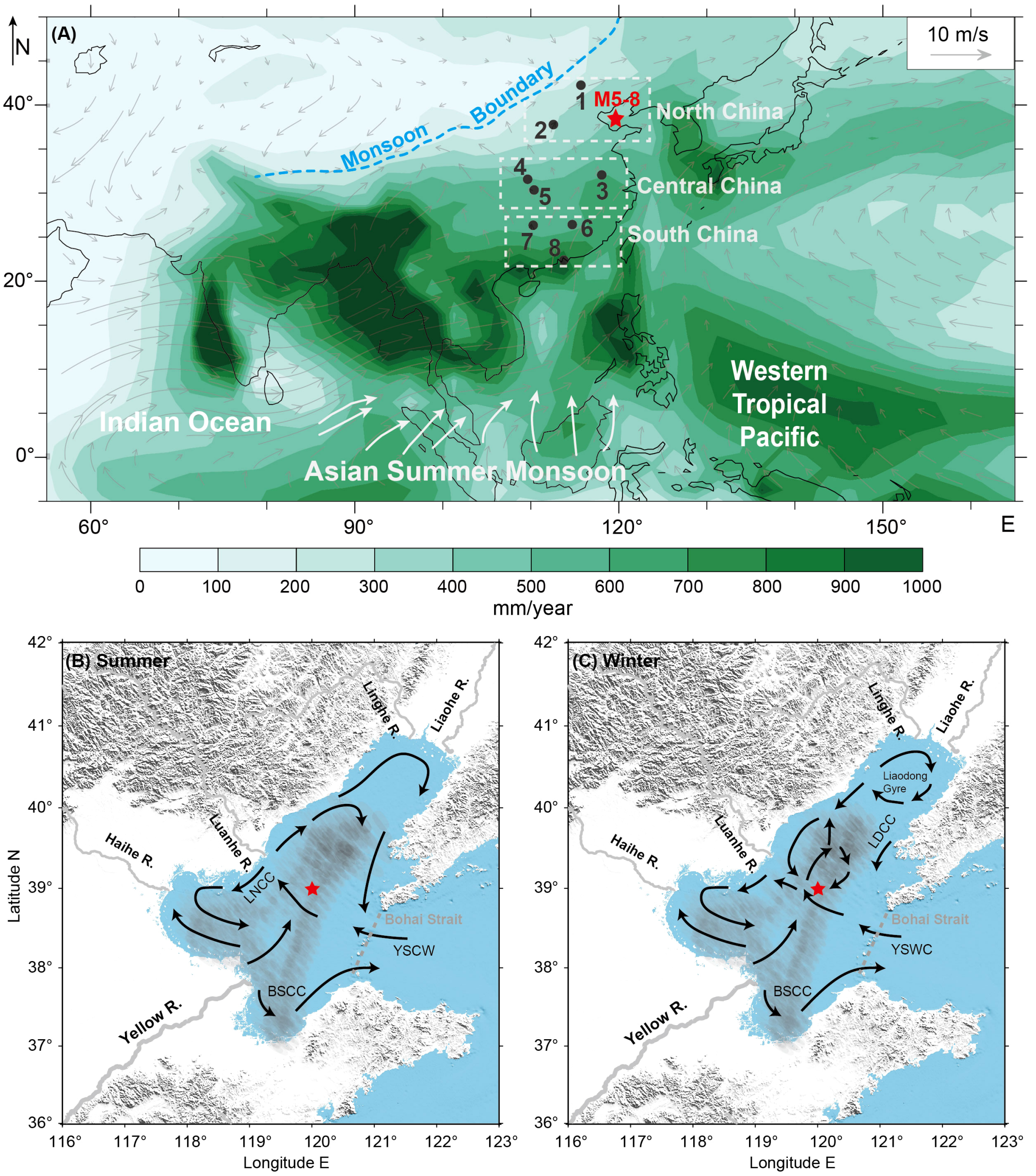

FIGURE 1
(A) Locations of the core M5-8 and other key sites are mentioned in the text, including 1: Dali Lake (Wen et al., 2017), 2: Gonghai Lake (Chen et al., 2015a), 3: Nvshan Lake (Jiang et al., 2021b), 4: Dajiuhu Peat (He et al., 2003), 5: Heshang Cave (Li et al., 2014), 6: core YHS (Zhao et al., 2024), 7: Daping Swamp (Zhong et al., 2017), 8: core DA (Zhang et al., 2024). The background shading represents the climatological summer (June-July-August) precipitation (unit: mm/year) from the GPCP data (Adler et al., 2003), while the black vectors depict the 850 hPa wind pattern (unit: m/s) from the NCEP Reanalysis II data over the Asia Summer Monsoon region (Kanamitsu et al., 2002). The data for both variables cover the period of 1979-2014 on a 2.5°×2.5° global grid. The monsoon boundary is modified from Zhou et al. (2016). The Ocean circulations in the Bohai Sea in summer **(B, C)** winter season (modified after Li et al., 2020). YSWC, Yellow Sea Warm Current; YSCW, Yellow Sea Cold Water; BSCC, Bohai Sea Coastal Current,; LNCC, Liaonan Coastal Current; LDCC, Liaodong Coastal Current. The red star indicates the position of core M5-8. The mud area (defined by mean grain size less than 16 μm) was delineated by gray lines (Qiao et al., 2017).

3.2 Grain-size and clay mineral analysis

For the grain-size analysis, a total of 159 bulk samples were pretreated using the H_2O_2-HCl procedure to remove organic matter and carbonates, respectively. Grain size frequency distributions were measured using a Malvern Mastersizer 3000G laser diffraction particle analyzer at the Centre for Marine Magnetism (CM^2), Southern University of Science and Technology, Shenzhen, China. Clay mineral studies were conducted on 15 samples of the <2 μm fraction, which was separated using Stoke's settling velocity principle (Dane et al., 2002), following the removal of organic matter and carbonate through treatment with 15% hydrogen peroxide and 25% acetic acid. Clay mineral assemblages were determined by X-ray diffraction using a D8 ADVANCE diffractometer with CuKα radiation (40kV, 40 mA) at the Key Laboratory of Marine Geology and Environment, Institute of Oceanology, Chinese Academy of Sciences, Qingdao, China.

3.3 Climate model simulations

To verify the variations in precipitation patterns over the past millennium, historical simulations in the National Center for Atmospheric Research (NCAR) Community Earth System Model Last Millennium Ensemble (CESM-LME) archive (Otto-Bliesner et al., 2016) are used for the period 850-1850 CE. The LME is a set of transient climate simulations that includes two categories: (1) an all-forcing experiment in which all transient forcings (including greenhouse gases, land-use changes, ozone, aerosols, and volcanic eruptions) are incorporated together, and (2) single-forcing simulations where each transient forcing factor is applied individually. In this study, we used the monthly precipitation and 850 hPa wind from the 13 all-forcing experiments, 4 solar radiation sensitivity experiments, and 5 volcanic eruption sensitivity experiments from the CESM-LME archive to investigate the spatial patterns of summer precipitation and the corresponding synoptic circulation. CESM-LME experiments were run with the Community Earth System Model version 1.1 with a horizontal resolution of 1.9×2.5 degrees. The forcing data used in CESM-LME as shown in Supplementary Table 1.

4 Results

4.1 Clay mineralogy and sediment provenance

The clay mineral assemblages of core M5-8, as shown in Supplementary Table 2, are dominated by illite, which constitutes 50.55 to 64.71% of the composition, with an average of 59.72%. Smectite (12.79-22.94%), kaolinite (9.52-13.17%), and chlorite (10.37-15.9%) are also present but in relatively lower proportions, with average contents of 16.16%, 11.14%, and 12.98%, respectively.

The Yellow River discharges approximately 0.7 billion tons of sediments annually into the surrounding oceans and is considered to be the primary source of sediment for the Bohai Sea (Qiao et al., 2017; Li et al., 2020). The composition of clay minerals indicate that the core M5-8 sediments mainly originated from the Yellow River (Figure 2), which is consistent with the provenance indicated by clay minerals in the surface sediments of the Bohai Sea (Yu et al., 2017). Furthermore, the distribution of heavy minerals and magnetic properties provides additional evidence supporting that the Yellow River is the main sediment source for the central basin of the Bohai Sea (Han et al., 2013; Li et al., 2020). Consequently, it can be reasonably inferred that the sediment of core M5-8 is predominantly derived from the Yellow River, which receives a substantial sediment supply from the Loess Plateau (Ren and Shi, 1986). This makes our site an ideal location to capture the variability of precipitation over the northern section of the tripole precipitation regime.

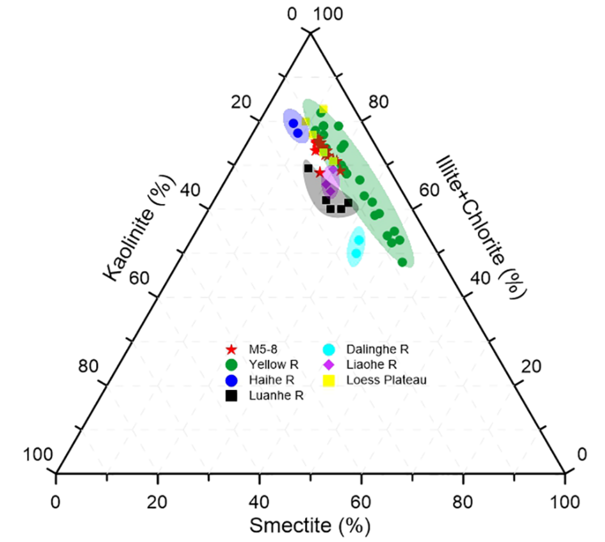

FIGURE 2
Provenance discrimination plot of clay minerals. The Yellow River data are from Zhang et al. (2019) and Yang et al. (2003), the Haihe, Luanhe, Dalinghe, and Liaohe Rivers data are from Dou et al. (2014), and the Loess Plateau data are from Zhang et al. (2019) and Ren and Shi (1986).

4.2 Grain size distribution and climate significance

Figure 3 displays the variation in grain size distribution for the sediment from core M5-8. The grain size frequency distribution curves and the grain size standard deviation model reveal a bimodal grain size structure (Figures 3A, B), probably suggesting the influence of two distinct hydrodynamics in the region. The main components of the sediments are silt (26.98-64.46%, with an average of 49.41%) and sand (21.67-66.78%, with an average of 42.12%). Minor amounts of clay are also present (4.85-14.25%, with an average of 8.47%).

Approximately 85% of the Yellow River's annual sediment load is discharged into the sea during the flood season, which occurs in the summer (Li et al., 1998). Seasonal variations in the intensity of the monsoon winds leads to corresponding changes in the hydrodynamic conditions of the Bohai Sea, with stronger hydrodynamic conditions during winter when the monsoon winds are intense and weaker conditions during summer when the monsoon winds are less intense (Figure 1, Wang et al., 2014; Yang et al., 2011). Coarse-grained sediments deposit near the Yellow River delta in summer and are resuspended and exported to the surrounding ocean in winter due to strong hydrodynamic conditions (Li et al., 2010; Wang et al., 2014), while fine-grained sediments are transported seaward in summer under weaker hydrodynamic conditions (Li et al., 2010; Meng et al., 2023).

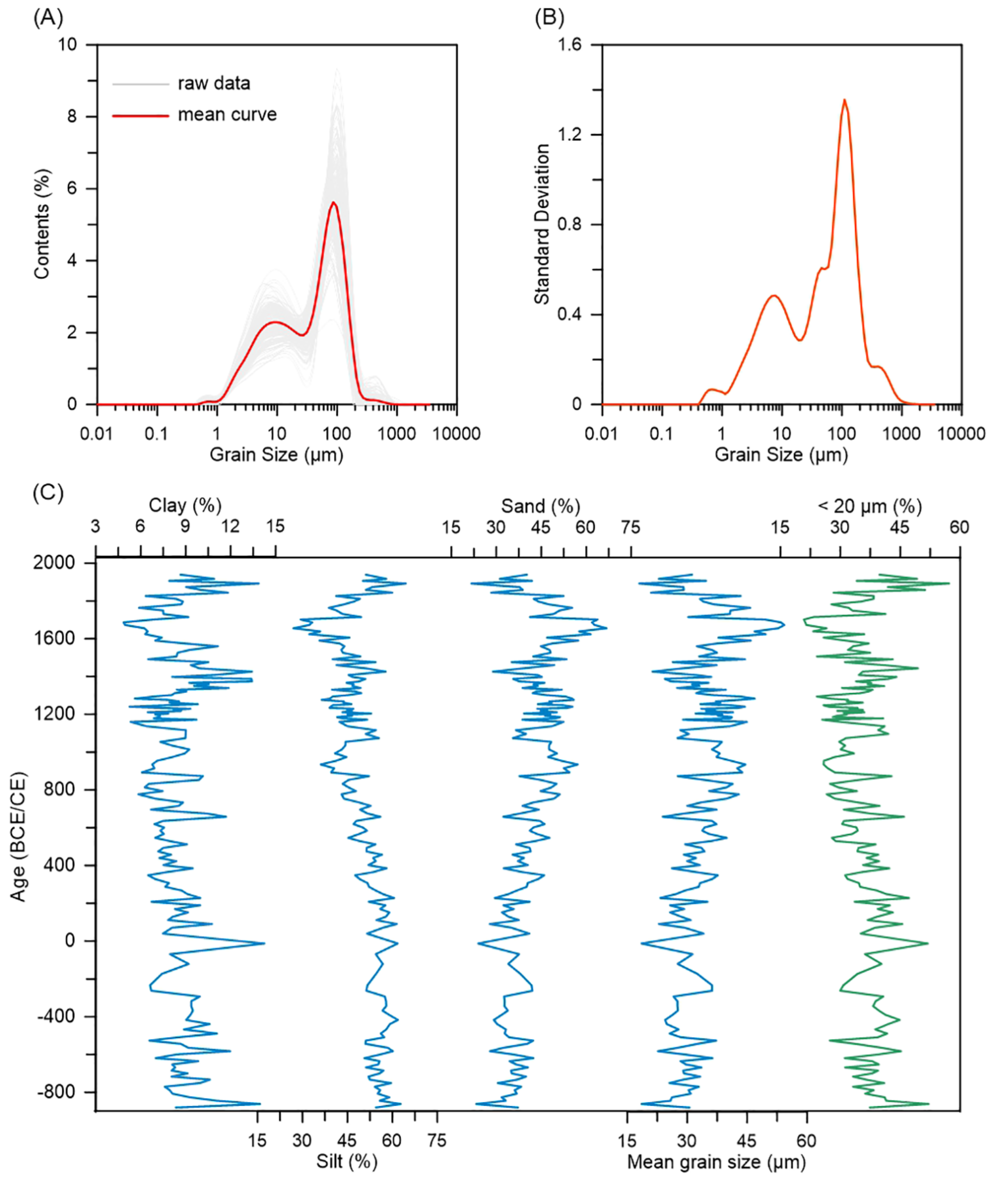

FIGURE 3
Sediment grain size results for core M5-8. **(A)** Grain size frequency distribution curves for all samples. **(B)** The grain size standard deviation model. **(C)** Variations in clay/silt/sand content, mean grain size, and the fine-grained fraction (<20 μm) since ~900 BCE.

Previous studies have shown that the Yellow River runoff is primarily governed by the ASM (Yi et al., 2012; Wu et al., 2020), indicating that fine-grained sediments can serve as a proxy for variations in ASM-driven precipitation. Data from the Lijin station over the past 70 years show a high correlation between the Yellow River's annual runoff and sediment load, both of which are also related to basin's summer precipitation (Supplementary Figure 2). This indicates that increased summer precipitation leads to higher runoff and sediment load, including the fine-grained sediment. Although certain indices were affected by the Yellow River diversion, the sediment grain size remains a reliable indicator of regional precipitation proxy (Zhou et al., 2013; Zhang et al., 2020). Under normal regional dynamic conditions, the fine-grained fraction of sediment (<20 μm, ~>5.6 φ) can be transported as suspended particles from rivers to the sea (Fan et al., 2002). In this study, we define the fine-grained fraction of <20 μm in core M5-8 as a proxy for the intensity of ASM.

4.3 The ASM variations during the late Holocene

The fine-grained sediments extracted from core M5-8 provide a high-resolution ASM precipitation record covering ~2900 years (Figure 4b). From ~900 BCE to around 1000 CE, there was a gradual decreasing trend in ASM precipitation. During the last millennium, ASM precipitation exhibited a notably high intensity between 1000 and 1300 CE, but was comparatively weak from 1450

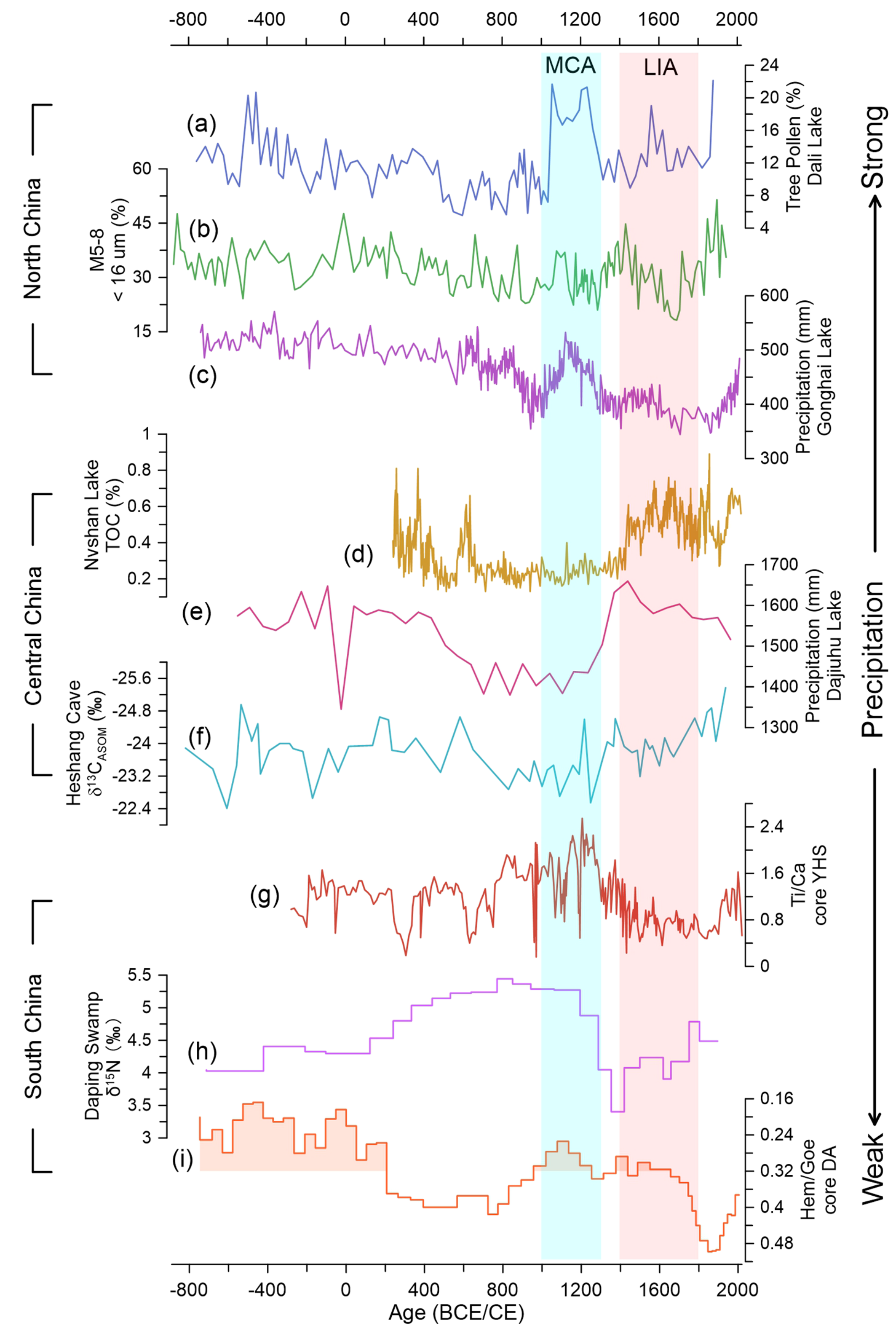

FIGURE 4
Comparison of Asian Summer Monsoon precipitation records from **(a)** Dali Lake at 43.26° (Wen et al., 2017), **(b)** core M5-8, **(c)** Gonghai Lake (Chen et al., 2015a), **(d)** Nvshan Lake (Jiang et al., 2021b), **(e)** Dajiuhu Peat (He et al., 2003), **(f)** Heshang Cave (Li et al., 2014), **(g)** core YHS (Zhao et al., 2024), **(h)** Daping Swamp (Zhong et al., 2017), **(i)** core DA (Zhang et al., 2024). MCA, Medieval Climate Anomaly; LIA, Little Ice Age.

to 1900 CE (Figure 4b). Our findings are generally consistent with other ASM studies carried out in North China (Figures 4a, c) within the bounds of chronological uncertainties (Chen et al., 2015a; Wen et al., 2017), which further confirms that our results accurately represent the regional behaviors of ASM precipitation.

On the other hand, the precipitation patterns in China exhibit significant spatial variations, especially during the last millennium (Figure 4). During the Medieval Climate Anomaly (MCA, 1000 - 1300 CE; IPCC, 2007), both the ASM records from North China (Figures 4a–c) and South China (Figures 4g–i) suggest a relatively wet condition. In contrast, the records from the Central China (Figures 4d, f) reveal a dry condition. However, during the Little Ice Age (LIA, 1400 - 1900 CE; IPCC, 2007), the aforementioned precipitation patterns were reversed (Figure 5). Consequently, these results indicate that a tripole precipitation pattern (i.e., "-/+/-" or "+/-/+") existed in eastern China during the last millennium.

5 Discussion

5.1 Influence factors of ASM precipitation in North China

Numerous studies have demonstrated that factors such as the migration of the ITCZ, ENSO, solar irradiance, etc. play significant

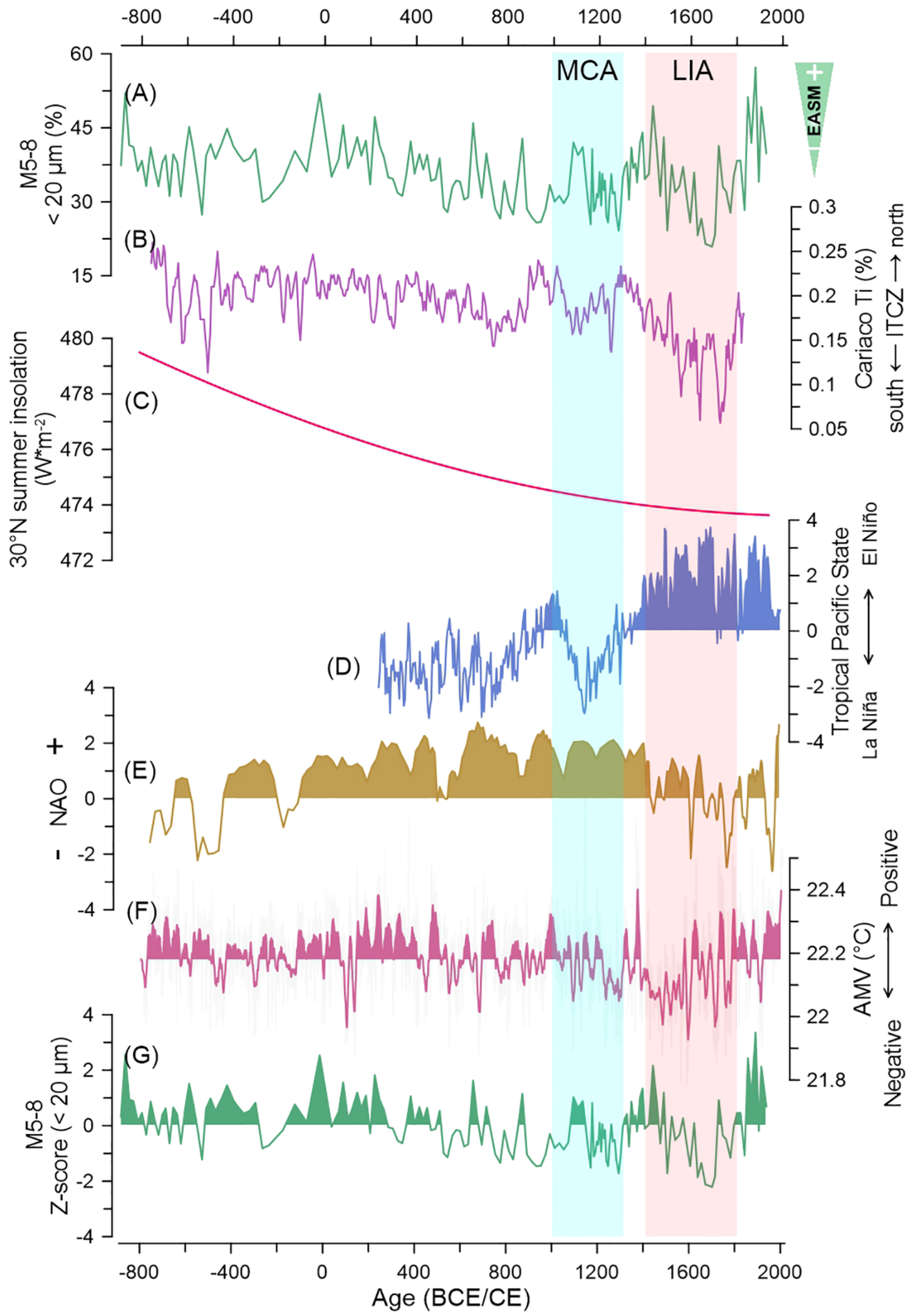

FIGURE 5
(A) Variation of fine-grained fraction from core M5-8. **(B)** Bulk Ti content of Cariaco Basin sediments from ODP Site 1002 (Haug et al., 2001). **(C)** 30° N summer insolation (Laskar et al., 2004). **(D)** Tropical Pacific mean-state index (Jiang et al., 2023b). **(E)** Mode of THE North Atlantic Oscillation (NAO) (Trouet et al., 2009; Olsen et al., 2012). **(F)** Variation of the Atlantic multidecadal variability (AMV) using a 15-year weight moving average window (purple) (Lapointe et al., 2020). **(G)** Z-score normalization curve for the fine-grained fraction from core M5-8.

roles in modulating precipitation variability in the ASM region, spanning across various timescales from interannual to millennial (e.g., Jiang et al., 2021b; Yancheva et al., 2007; Zhang et al., 2021). As shown in Figure 5, a positive correlation is observed between our ASM record (Figure 5B), 30°N summer insolation (Figure 5C), and especially the migration of the ITCZ. This suggests that the southward migration of the ITCZ directly contributed to the reduction in precipitation decrease in North China since ~900 BCE by weakening the ASM.

In terms of the internal variability of the climate system, the impact of ENSO on summer precipitation appears to have been more significant in the last millennium than in previous periods (Figures 5A, D). The WPSH is considered instrumental in facilitating the impact of ENSO on precipitation variations in eastern China (Chen et al., 2015b; Jiang et al., 2021b). A La Niña (El Niño) state would result in a strengthening and southwestward (weakening and northeastward) shift of the WPSH, as well as a strengthening (weakening) of the ASM (Ong-Hua and Feng, 2011). These changes in atmospheric circulation patterns contribute to an intensification (diminishment) of precipitation over North China (Rao et al., 2016b; He et al., 2017). Consequently, the observed increase (decrease) in North China precipitation during the MCA (LIA) can be influenced by the La Niña (El Niño) state (Figures 5A, D).

In addition to the low-latitude variability, the contribution of mid- and high-latitude variability, such as NAO and AMV, to ASM precipitation should not be ignored. The signals of the NAO are transmitted to East Asia via stationary waves and influence the summer precipitation in the region (Linderholm et al., 2011). However, our ASM record displays no significant correlation with the variations in the NAO mode during the late Holocene (Figures 5A, E, G), which is inconsistent with the weather station data (Sung et al., 2006). Conversely, our ASM record demonstrates a robust positive correlation with AMV, consistent with the modern observations and ensemble experiments (Lu et al., 2006; Wang et al., 2009), where high summer precipitation corresponds to the warm AMV phase and vice versa (Figures 5F, G). This enhanced ASM precipitation during the warm AMV phase is due to the coupled atmosphere-ocean feedback in the western Pacific and Indian Oceans as well as the circum-global teleconnection wave train pattern over Eurasia (Lu et al., 2006). Similarly, Gao et al. (2017) proposed that compared to other climate drivers like NAO and PDO, AMV has been the dominant forcing factor on monsoon and extreme precipitation in the ASM region over the past few decades.

Overall, our data indicates that southward ITCZ migration has led to reduced precipitation in North China since ~900 CE. Superimposed on this long-term trend, the AMV modulates precipitation, with warm phases potentially enhancing it and cold phases reducing it.

5.2 External forcings contributing to the tripole precipitation pattern in eastern China

The ASM precipitation records in eastern China reveal a tripole precipitation pattern over the last millennium (Figure 4). This finding differ from previous studies that identified dipole or alternating dipole and tripole structures (Chen et al., 2015b; Wang et al., 2022). Previous studies suggested that the dominant factors influencing summer precipitation patterns in eastern China were ENSO or the coupled PDO, AMV, and ASM (e.g., Chen et al., 2015b; Wang et al., 2022). However, external forcings such as solar radiation and volcanic activity have undergone significant changes over the past thousand years (Crowley, 2000; Mann et al., 2009). These distinct variations in external forcing give rise to diverse atmospheric circulation patterns, ocean-atmosphere interactions, and sea surface temperature (SST) modes, ultimately leading to obvious spatial variations in precipitation (Otterå et al., 2010; Man and Zhou, 2011; Liu et al., 2014). Additionally, internal forcings like ENSO, PDO, and AMO can be modulated by solar radiation and/or volcanic activity, thereby influencing the ASM precipitation (Paik et al., 2020; Liu et al., 2022; Sun et al., 2022; Du et al., 2023). The impact of external forcing factors such as solar radiation on ASM is amplified through internal forcing factors (Du et al., 2023). Consequently, it is unlikely that internal forcings played a major role in determining the summer precipitation patterns in eastern China. Instead, they were probably primarily modulated by external forcings. Therefore, we employed numerical experiments using the CESM-LME (Otto-Bliesner et al., 2016) to investigate the impact of external forcing on the tripole precipitation pattern in eastern China.

The numerical model results reveal a distinct tripole precipitation pattern in eastern China during the MCA and LIA (Figures 6A, B), demonstrating remarkable concordance with precipitation records (Figure 4). During the MCA, intensified solar radiation strengthens the ASM, inducing cyclonic circulation over South China and anti-cyclonic circulation over North China. These were achieved through both direct influences of the ITCZ northern shift and indirect influences of the circum-global teleconnection wave train through a positive AMV-like phase (Zhang et al., 2018; Qin et al., 2022), leading to divergence over Central China (Figure 6A). These circulation anomalies lead to an increase in precipitation in both South and North China, while suppressing precipitation in Central China (Figure 6A). Conversely, during the LIA, reduced solar radiation and increased volcanic activity weakened the ASM, leading to convergence over Central China (Figure 6B), due to the southern shift of the ITCZ and the negative AMV-like phase. Consequently, these altered circulation anomalies result in a reversal of the precipitation pattern compared to the MCA (Figure 6B).

To understand the drivers of these changes, we used the single forcing simulations of the CESM-LME. The solar radiation sensitivity experiment shows a relatively weak tripole structure, with wetter conditions over North China and South China and drier conditions in Central China during the MCA and the opposite during the LIA (Figures 6E, F). However, the drying/wetting of Central China is relatively weak and displaced northward compared to the all-forcing simulation (Figures 6A, B). Meanwhile, the volcanic forcing sensitivity experiment shows MCA drying and LIA wetting patterns over Central China that are similar to those in the full forcing simulation (Figures 6C, D). Furthermore, the differences between MCA and LIA from solar activity and volcanic eruption sensitivity experiments are not exactly the same

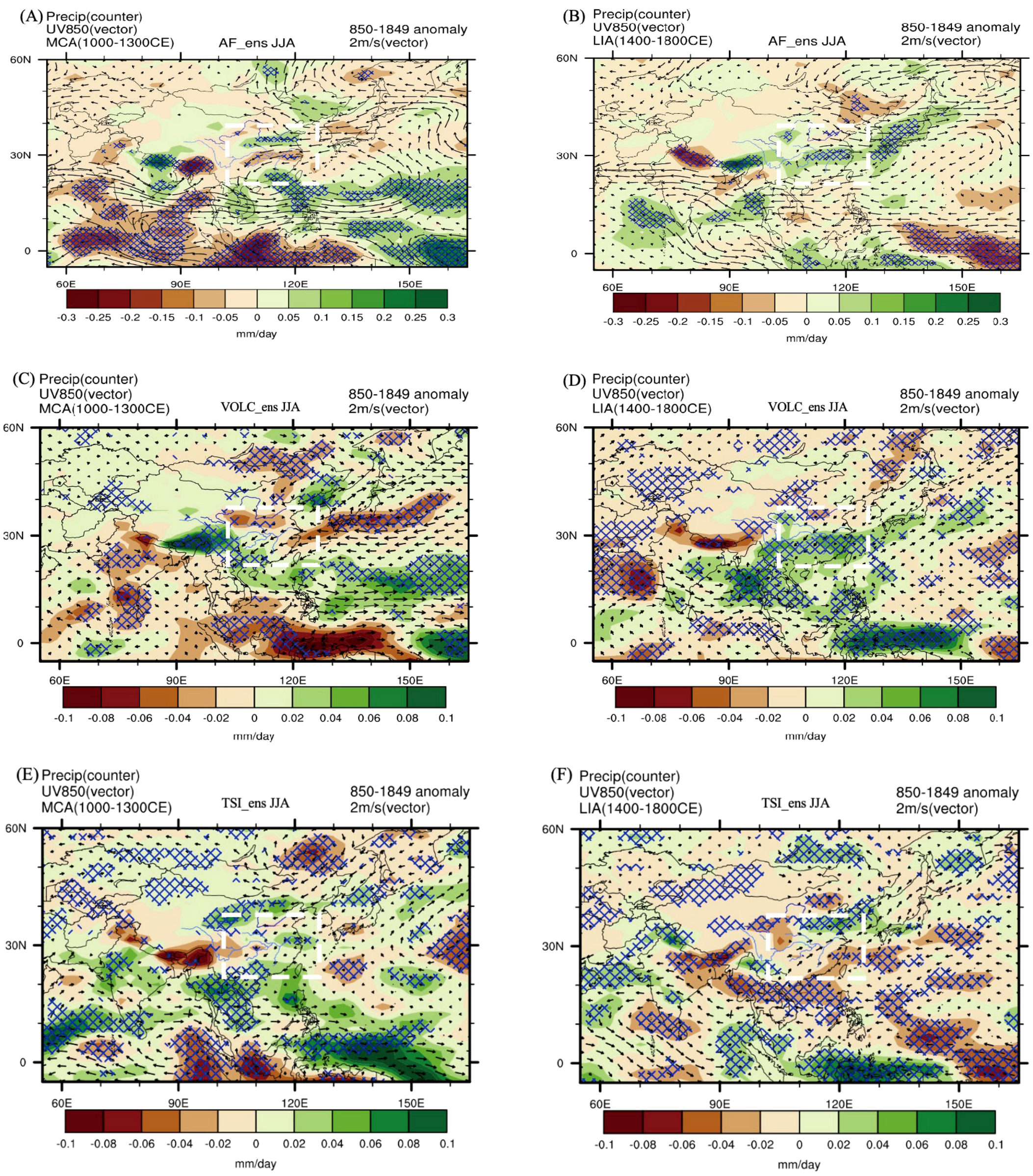

FIGURE 6
Spatial distributions of summer (June to August) precipitation anomalies (shade, unit: mm/day) and 850hPa wind anomalies (vector, unit: m/s) during the MCA **(A, C, E)** and LIA **(B, D, F)** from CESM-LME all-forcing experiments **(A, B)**, volcanic eruption sensitivity experiments **(C, D)**, and solar radiation sensitivity experiments **(E, F)**. The region marked by the dashed line represents eastern China. The blue grid indicates 90% confidence.

as in the all-forcing experiments (Supplementary Figure 3). These results indicate that the tripole pattern in precipitation was not solely determined by one factor, but rather by the combined effects of solar radiation and volcanic activity.

In addition, external forcings contribute significantly to the SST patterns by directly influencing the tropical SST (Jiang et al., 2023a; Otterå et al., 2010), thereby impacting the monsoon precipitation variability in eastern China (Chen et al., 2015b; Jiang et al., 2021b). Intense (weak) solar radiation and weak (intense) volcanic eruptions could cause the tropical Pacific to become similar to a La Niña (El Niño) anomaly through the ocean dynamical thermostat mechanism (Clement et al., 1996; Jiang et al., 2023a). As a result, this leads to more (less) precipitation in North and South China, and less (more) precipitation in Central China (He et al., 2017; Jiang et al., 2021b).

In summary, the combined influences of solar radiations and volcanic eruptions on ASM precipitation over eastern China are achieved through direct influences on circulation patterns and indirect influences on internal variability, such as AMV and ENSO. In the face of increasing greenhouse gas emissions and climate warming, we proposed that eastern China may experience a tripole precipitation structure on the centennial scale, with a potential trend of increasing precipitation in North China (Jiang et al., 2021a; You and Wang, 2021).

6 Conclusions

This study reconstructs a ~2900-year ASM precipitation record for North China based on grain-size and clay mineral analyses of core M5-8 retrieved from the Bohai Sea, China. The sediment source is predominantly the Yellow River, with fine-grained particles serving as a proxy for ASM precipitation. Our results demonstrate that southward migration of the ITCZ has driven long-term reduced precipitation in North China, with the AMV superimposing fluctuations through atmosphere-ocean feedback and circum-global teleconnection. Furthermore, a synthesis of paleoclimate records from eastern China over the last millennium reveals a tripole precipitation pattern, characterized by a positive-negative-positive (negative-positive-negative) structure in North, Central, and South China during MCA (LIA), respectively. CESM-LME simulations establish that this summer precipitation pattern arose from the combined effects of solar radiation variations and volcanic forcing, which directly modulated circulation patterns and indirectly influenced internal variability, including AMV and ENSO.

Data availability statement

The original contributions presented in the study are included in the article/Supplementary Material. Further inquiries can be directed to the corresponding authors.

Author contributions

HL: Writing – original draft. JT: Writing – review & editing. YZ: Writing – review & editing. LN: Methodology, Writing – review & editing. JL: Writing – review & editing. CS: Writing – review & editing. WZ: Formal Analysis, Writing – review & editing. Y-MC: Supervision, Writing – review & editing. QL: Supervision, Writing – review & editing.

Funding

The author(s) declare that financial support was received for the research, authorship, and/or publication of this article. This work was supported by the National Natural Science Foundation of China (42261144739, 42176066, 42274094, 42474097), State Key Laboratory of Marine Geology, Tongji University (No. MGK202209).

Conflict of interest

The authors declare that the research was conducted in the absence of any commercial or financial relationships that could be construed as a potential conflict of interest.

Generative AI statement

The author(s) declare that no Generative AI was used in the creation of this manuscript.

Publisher's note

Supplementary material

The Supplementary Material for this article can be found online at: https://www.frontiersin.org/articles/10.3389/fmars.2025.1556480/full#supplementary-material

References

Adler, R. F., Huffman, G. J., Chang, A., Ferraro, R., Xie, P. P., Janowiak, J., et al. (2003). The version-2 global precipitation climatology project (GPCP) monthly precipitation analysis-present). *J. Hydrometeorol.* 4, 1147–1167. doi: 10.1175/1525-7541(2003)004<1147:TVGPCP>2.0.CO;2

Chen, F., Xu, Q., Chen, J., Birks, H. J. B., Liu, J., Zhang, S., et al. (2015a). East Asian summer monsoon precipitation variability since the last deglaciation. *Sci. Rep.* 5, 11186. doi: 10.1038/srep11186

Cheng, H., Edwards, R. L., Sinha, A., Spötl, C., Yi, L., Chen, S., et al. (2016). The Asian monsoon over the past 640,000 years and ice age terminations. *Nature* 534, 640–646. doi: 10.1038/nature18591

Chen, J., Chen, F., Feng, S., Huang, W., Liu, J., and Zhou, A. (2015b). Hydroclimatic changes in China and surroundings during the Medieval Climate Anomaly and Little Ice Age: Spatial patterns and possible mechanisms. *Quat. Sci. Rev.* 107, 98–111. doi: 10.1016/j.quascirev.2014.10.012

Chen, K., Ning, L., Liu, Z., Liu, J., Yan, M., Sun, W., et al. (2020). One drought and one volcanic eruption influenced the history of China: the late ming dynasty mega-drought. *Geophys. Res. Lett.* 47, 1–9. doi: 10.1029/2020GL088124

Clement, A. C., Seager, R., Cane, M. A., and Zebiak, S. E. (1996). An ocean dynamical thermostat. *J. Clim.* 9, 2190–2196. doi: 10.1175/1520-0442(1996)009<2190:AODT>2.0.CO;2

Crowley, T. J. (2000). Causes of climate change over the past 1000 years. *Sci. (80-.).* 289, 270–277. doi: 10.1126/science.289.5477.270

Dai, G., Zhang, Z., Otterå, O. H., Langebroek, P. M., Yan, Q., and Zhang, R. (2021). A modeling study of the tripole pattern of east China precipitation over the past 425 ka. *J. Geophys. Res. Atmos.* 126, 1–13. doi: 10.1029/2020JD033513

Dane, J. H., Topp, C., Campbell, G. S., Horton, R., Jury, W. A., Nielsen, D. R., et al. (2002). Part 4. Physical methods. Methods of soil analysis. . *Soil Sci. Soc Am. Madison WI U.S.A.* doi: 10.2136/sssabookser5.4

Ding, Y., Sun, Y., Wang, Z., Zhu, Y., and Song, Y. (2009). Inter-decadal variation of the summer precipitation in China and its association with decreasing Asian summer monsoon Part II: Possible causes. *Int. J. Climatol.* 29, 1926–1944. doi: 10.1002/joc.1759

Ding, Y., Wang, Z., and Sun, Y. (2008). Inter-decadal variation of the summer precipitation in East China and its association with decreasing Asian summer monsoon. Part I: Observed evidences. *Int. J. Climatol.* 28, 1139–1161. doi: 10.1002/joc.1615

Dou, Y., Li, J., Zhao, J., Wei, H., Yang, S., Bai, F., et al. (2014). Clay mineral distributions in surface sediments of the Liaodong Bay, Bohai Sea and surrounding river sediments: Sources and transport patterns. *Cont. Shelf Res.* 73, 72–82. doi: 10.1016/j.csr.2013.11.023

Du, X., Dee, S., Hu, J., and Thirumalai, K. (2023). Solar irradiance modulates the asian summer monsoon—ENSO relationship over the last millennium. *Geophys. Res. Lett.* 50, 1–11. doi: 10.1029/2023GL105708

Fan, D., Yang, Z., Sun, X., Zhang, D., and Guo, Z. (2002). Quantitative evaluation of sediment provenance on the north area of the East China Sea shelf. *J. Ocean Univ. Qingdao* 32, 748–756.

Fang, Y., Fang, G., and Zhang, Q. (2000). Numerical simulation and dynamic study of the wintertime circulation of the Bohai Sea. *Chin. J. Oceanol. Limnol.* 18, 1–9. doi: 10.1007/BF02842535

Gao, T., Wang, H. J., and Zhou, T. (2017). Changes of extreme precipitation and nonlinear influence of climate variables over monsoon region in China. *Atmos. Res.* 197, 379–389. doi: 10.1016/j.atmosres.2017.07.017

Han, Z.-Z., Hong, Y. W., Li, M., Zhang, J.-Q., and Zou, H. (2013). Analysis for heavy mineral characteristics and material provenance in the sediments of the Northern. *Period. Ocean Univ. China* 43, 73–79.

Haug, G. H., Hughen, K. A., Sigman, D. M., and Peterson, L. C. (2001). Southward migration of the intertropical convergence zone through the holocene. *Sci. (80-.).* 293, 1304–1308. doi: 10.1126/science.1059725

He, B., Zhang, S., and Cai, S. (2003). Climatic changes recorded in peat from the Dajiu lake basin in Shennongjia since the last 2600 years. *Mar. Geol. Quat. Geol.* 23, 109–116.

He, C., Lin, A., Gu, D., Li, C., Zheng, B., and Zhou, T. (2017). Interannual variability of Eastern China Summer Rainfall: the origins of the meridional triple and dipole modes. *Clim. Dyn.* 48, 683–696. doi: 10.1007/s00382-016-3103-x

Jiang, R., Sun, L., Sun, C., and Liang, X. Z. (2021a). and understanding of China precipitation projections. *Clim. Dyn.* 57, 1079–1096. doi: 10.1007/s00382-021-05759-z

Jiang, L., Yu, K., Tao, S., Li, Y., and Wang, S. (2023a). Abrupt increase in ENSO variability at 700 CE triggered by solar activity. *J. Geophys. Res. Ocean.* 128, 1–12. doi: 10.1029/2022JC019278

Jiang, S., Zhou, X., Sachs, J. P., Li, Z., Tu, L., Lin, Y., et al. (2023b). The mean state of the tropical Pacific Ocean differed between the Medieval Warm Period and the Industrial Era. *Commun. Earth Environ.* 4, 74. doi: 10.1038/s43247-023-00734-4

Jiang, S., Zhou, X., Sachs, J. P., Luo, W., Tu, L., Liu, X., et al. (2021b). Central eastern China hydrological changes and ENSO-like variability over the past 1800 yr. *Geology* 49, 1386–1390. doi: 10.1130/G48894.1

Kanamitsu, M., Ebisuzaki, W., Woollen, J., Yang, S., Hnilo, J. J., Fiorino, M., et al. (2002). NCEP–DOE AMIP-II reanalysis (R-2). *Bull. Am. Meteorol. Soc* 83, 1631–1644. doi: 10.1175/BAMS-83-11-1631

Lapointe, F., Bradley, R. S., Francus, P., Balascio, N. L., Abbott, M. B., Stoner, J. S., et al. (2020). Annually resolved Atlantic sea surface temperature variability over the past 2,900 y. *Proc. Natl. Acad. Sci. U. S. A.* 117, 27171–27178. doi: 10.1073/pnas.2014166117

Laskar, J., Robutel, P., Joutel, F., Gastineau, M., Correia, A. C. M., and Levrard, B. (2004). A long-term numerical solution for the insolation quantities of the Earth. *Astron. Astrophys.* 428, 261–285. doi: 10.1051/0004-6361:20041335

Li, X., Hu, C., Huang, J., Xie, S., and Baker, A. (2014). A 9000-year carbon isotopic record of acid-soluble organic matter in a stalagmite from Heshang Cave, central China: Paleoclimate implications. *Chem. Geol.* 388, 71–77. doi: 10.1016/j.chemgeo.2014.08.029

Li, H., Tang, J., Gai, C., Zhang, W., Humbert, F., Ni, Y., et al. (2023). Persistent influence of non-dipole geomagnetic field on east asia over the past 4,000 years. *J. Geophys. Res. Solid Earth* 128, 1–17. doi: 10.1029/2023JB027359

Li, G., Wang, H., and Liao, H. (2010). Numerical simulation on seasonal transport variations and mechanisms of suspended sediment discharged from the Yellow River to the Bohai Sea. *J. Geogr. Sci.* 20, 923–937. doi: 10.1007/s11442-010-0821-6

Li, G., Wei, H., Han, Y., and Chen, Y. (1998). Sedimentation in the Yellow River delta, Part I: Flow and suspended sediment structure in the upper distributary and the estuary. *Mar. Geol.* 149, 93–111. doi: 10.1016/S0025-3227(98)00031-0

Li, M., Zhu, S., Ouyang, T., Tang, J., and He, C. (2020). Magnetic fingerprints of surface sediment in the Bohai Sea, China. *Mar. Geol.* 427, 106226. doi: 10.1016/j.margeo.2020.106226

Linderholm, H. W., Ou, T., Jeong, J. H., Folland, C. K., Gong, D., Liu, H., et al. (2011). Interannual teleconnections between the summer North Atlantic Oscillation and the East Asian summer monsoon. *J. Geophys. Res. Atmos.* 116, 1–13. doi: 10.1029/2010JD015235

Liu, F., Gao, C., Chai, J., Robock, A., Wang, B., Li, J., et al. (2022). Tropical volcanism enhanced the East Asian summer monsoon during the last millennium. *Nat. Commun.* 13 (1), 3429. doi: 10.1038/s41467-022-31108-7

Liu, Z., Lu, Z., Wen, X., Otto-Bliesner, B. L., Timmermann, A., and Cobb, K. M. (2014). Evolution and forcing mechanisms of El Niño over the past 21,000 years. *Nature* 515, 550–553. doi: 10.1038/nature13963

Lougheed, B. C., and Obrochta, S. P. (2019). A rapid, deterministic age-depth modeling routine for geological sequences with inherent depth uncertainty. *Paleoceanogr. Paleoclimatology* 34, 122–133. doi: 10.1029/2018PA003457

Lu, R., Dong, B., and Ding, H. (2006). Impact of the Atlantic Multidecadal Oscillation on the Asian summer monsoon. *Geophys. Res. Lett.* 33, L24701. doi: 10.1029/2006GL027655

Man, W. M., and Zhou, T. J. (2011). Forced response of atmospheric oscillations during the last millennium simulated by a climate system model. *Chin. Sci. Bull.* 56, 3042–3052. doi: 10.1007/s11434-011-4637-2

Mann, M. E., Zhang, Z., Rutherford, S., Bradley, R. S., Hughes, M. K., Shindell, D., et al. (2009). Global signatures and dynamical origins of the little ice age and medieval climate anomaly. *Sci. (80-.).* 326, 1256–1260. doi: 10.1126/science.1177303

Meng, L., Wang, L., Zhao, J., Zhan, C., Liu, X., Cui, B., et al. (2023). End-member characteristics of sediment grain size in modern Yellow River delta sediments and its environmental significance. *Front. Mar. Sci.* 10. doi: 10.3389/fmars.2023.1141187

Olsen, J., Anderson, N. J., and Knudsen, M. F. (2012). Variability of the North Atlantic Oscillation over the past 5,200 years. *Nat. Geosci.* 5, 808–812. doi: 10.1038/ngeo1589

Ong-Hua, S., and Feng, X. (2011). Two northward jumps of the summertime western pacific subtropical high and their associations with the tropical SST anomalies. *Atmos. Ocean. Sci. Lett.* 4, 98–102. doi: 10.1080/16742834.2011.11446910

Otterå, O. H., Bentsen, M., Drange, H., and Suo, L. (2010). External forcing as a metronome for Atlantic multidecadal variability. *Nat. Geosci.* 3, 688–694. doi: 10.1038/ngeo955

Otto-Bliesner, B. L., Brady, E. C., Fasullo, J., Jahn, A., Landrum, L., Stevenson, S., et al. (2016). Climate variability and change since 850 CE: an ensemble approach with the community earth system model. *Bull. Am. Meteorol. Soc* 97, 735–754. doi: 10.1175/BAMS-D-14-00233.1

Paik, S., Min, S. K., Iles, C. E., Fischer, E. M., and Schurer, A. P. (2020). Volcanic-induced global monsoon drying modulated by diverse El Ninõ responses. *Sci. Adv.* 6, 1–8. doi: 10.1126/sciadv.aba1212

Porter, S. C., and An, Z. (1995). Correlation between climate events in the North Atlantic and China during the last glaciation. *Nature* 375, 305–308. doi: 10.1038/375305a0

Qiao, S., Shi, X., Wang, G., Zhou, L., Hu, B., Hu, L., et al. (2017). Sediment accumulation and budget in the Bohai Sea, Yellow Sea and East China Sea. *Mar. Geol.* 390, 270–281. doi: 10.1016/j.margeo.2017.06.004

Qin, Y., Ning, L., Li, L., Liu, Z., Liu, J., Yan, M., et al. (2022). Assessing the modern multi-decadal scale aridification over the northern China from a historical perspective. *J. Geophys. Res. Atmos.* 127, 1–17. doi: 10.1029/2021JD035622

Rao, Z., Jia, G., Li, Y., Chen, J., Xu, Q., and Chen, F. (2016a). Asynchronous evolution of the isotopic composition and amount of precipitation in north China during the Holocene revealed by a record of compound-specific carbon and hydrogen isotopes of long-chain n-alkanes from an alpine lake. *Earth Planet. Sci. Lett.* 446, 68–76. doi: 10.1016/j.epsl.2016.04.027

Rao, Z., Li, Y., Zhang, J., Jia, G., and Chen, F. (2016b). Investigating the long-term palaeoclimatic controls on the δ D and δ 18 O of precipitation during the Holocene in the Indian and East Asian monsoonal regions. *Earth-Science Rev.* 159, 292–305. doi: 10.1016/j.earscirev.2016.06.007

Ren, M., and Shi, Y. (1986). Sediment discharge of the Yellow River and its effect on sedimentation of the Bohai and Yellow Sea. *Sci. Geogr. Sin.* 6, 1–12. doi: 10.1016/0278-4343(86)90037-3

Sun, W., Liu, J., Wang, B., Chen, D., and Gao, C. (2022). Pacific multidecadal (50–70 year) variability instigated by volcanic forcing during the Little Ice Agamp]] ndash;1850). *Clim. Dyn.* 59, 231–244. doi: 10.1007/s00382-021-06127-7

Sung, M.-K., Kwon, W.-T., Baek, H.-J., Boo, K.-O., Lim, G.-H., and Kug, J.-S. (2006). A possible impact of the North Atlantic Oscillation on the east Asian summer monsoon precipitation. *Geophys. Res. Lett.* 33, L21713. doi: 10.1029/2006GL027253

Trouet, V., Esper, J., Graham, N. E., Baker, A., Scourse, J. D., and Frank, D. C. (2009). Persistent positive north atlantic oscillation mode dominated the medieval climate anomaly. *Sci. (80-.).* 324, 78–80. doi: 10.1126/science.1166349

Wang, Y. J., Cheng, H., Edwards, R. L., An, Z. S., Wu, J. Y., Shen, C.-C., et al. (2001). A high-resolution absolute-dated late pleistocene monsoon record from hulu cave, China. *Sci. (80-.).* 294, 2345–2348. doi: 10.1126/science.1064618

Wang, Y., Cheng, H., Edwards, R. L., Kong, X., Shao, X., Chen, S., et al. (2008). Millennial- and orbital-scale changes in the East Asian monsoon over the past 224,000 years. *Nature* 451, 1090–1093. doi: 10.1038/nature06692

Wang, M., Hu, C., Liu, Y., Li, L., Xie, S., and Johnson, K. (2022). Precipitation in eastern China over the past millennium varied with large-scale climate patterns. *Commun. Earth Environ.* 3, 321. doi: 10.1038/s43247-022-00664-7

Wang, Y., Li, S., and Luo, D. (2009). Seasonal response of Asian monsoonal climate to the Atlantic Multidecadal Oscillation. *J. Geophys. Res.* 114, D02112. doi: 10.1029/2008JD010929

Wang, J., Shen, Y., and Guo, Y. (2010). Seasonal circulation and influence factors of the Bohai Sea: A numerical study based on Lagrangian particle tracking method. *Ocean Dyn.* 60, 1581–1596. doi: 10.1007/s10236-010-0346-7

Wang, H., Wang, A., Bi, N., Zeng, X., and Xiao, H. (2014). Seasonal distribution of suspended sediment in the Bohai Sea, China. *Cont. Shelf Res.* 90, 17–32. doi: 10.1016/j.csr.2014.03.006

Wang, P. X., Wang, B., Cheng, H., Fasullo, J., Guo, Z. T., Kiefer, T., et al. (2017). The global monsoon across time scales: Mechanisms and outstanding issues. *Earth-Science Rev.* 174, 84–121. doi: 10.1016/j.earscirev.2017.07.006

Wang, J., Yang, B., Ljungqvist, F. C., and Zhao, Y. (2013). The relationship between the Atlantic Multidecadal Oscillation and temperature variability in China during the last millennium. *J. Quat. Sci.* 28, 653–658. doi: 10.1002/jqs.2658

Wen, R., Xiao, J., Fan, J., Zhang, S., and Yamagata, H. (2017). Pollen evidence for a mid-Holocene East Asian summer monsoon maximum in northern China. *Quat. Sci. Rev.* 176, 29–35. doi: 10.1016/j.quascirev.2017.10.008

Wu, X., Wang, H., Bi, N., Saito, Y., Xu, J., Zhang, Y., et al. (2020). Climate and human battle for dominance over the Yellow River's sediment discharge: From the Mid-Holocene to the Anthropocene. *Mar. Geol.* 425, 106188. doi: 10.1016/j.margeo.2020.106188

Yancheva, G., Nowaczyk, N. R., Mingram, J., Dulski, P., Schettler, G., Negendank, J. F. W., et al. (2007). Influence of the intertropical convergence zone on the East Asian monsoon. *Nature* 445, 74–77. doi: 10.1038/nature05431

Yang, Z., Ji, Y., Bi, N., Lei, K., and Wang, H. (2011). Sediment transport off the Huanghe (Yellow River) delta and in the adjacent Bohai Sea in winter and seasonal comparison. *Estuar. Coast. Shelf Sci.* 93, 173–181. doi: 10.1016/j.ecss.2010.06.005

Yang, S. Y., Jung, H. S., Lim, D., and Li, C. X. (2003). A review on the provenance discrimination of sediments in the Yellow Sea. *Earth-Science Rev.* 63, 93–120. doi: 10.1016/S0012-8252(03)00033-3

Yi, L., Yu, H. J., Ortiz, J. D., Xu, X. Y., Chen, S. L., Ge, J. Y., et al. (2012). Late Quaternary linkage of sedimentary records to three astronomical rhythms and the Asian monsoon, inferred from a coastal borehole in the south Bohai Sea, China. *Palaeogeogr. Palaeoclimatol. Palaeoecol.* 329-330, 329–330. doi: 10.1016/j.palaeo.2012.02.020

You, J., and Wang, S. (2021). Higher probability of occurrence of hotter and shorter heat waves followed by heavy rainfall. *Geophys. Res. Lett.* 48, 1–11. doi: 10.1029/2021GL094831

Yu, Y., Wang, Y., Li, R., Meng, X., Wang, Y., Dou, Z., et al. (2017). Clay minerals distribution pattern in surface sediments of western Bohai and their provenance implications. *Mar. Geol. Quat. Geol.* 37, 51–58. doi: 10.16562/j.cnki.0256-1492.2017.01.006

Zhang, H., Cheng, H., Sinha, A., Spötl, C., Cai, Y., Liu, B., et al. (2021). Collapse of the Liangzhu and other Neolithic cultures in the lower Yangtze region in response to climate change. *Sci. Adv.* 7, 1–10. doi: 10.1126/sciadv.abi9275

Zhang, Z., Sun, X., and Yang, X. Q. (2018). Understanding the interdecadal variability of East Asian summer monsoon precipitation: Joint influence of three oceanic signals. *J. Clim.* 31, 5485–5506. doi: 10.1175/JCLI-D-17-0657.1

Zhang, J., Wan, S., Clift, P. D., Huang, J., Yu, Z., Zhang, K., et al. (2019). History of Yellow River and Yangtze River delivering sediment to the Yellow Sea since 3.5 Ma: Tectonic or climate forcing? *Quat. Sci. Rev.* 216, 74–88. doi: 10.1016/j.quascirev.2019.06.002

Zhang, T., Yang, X., Yin, J., Chen, Q., Hu, J., Wang, L., et al. (2024). Low-latitude hydroclimate changes related to paleomagnetic variations during the Holocene in coastal southern China. *Front. Earth Sci.* 18. doi: 10.1007/s11707-022-1009-y

Zhang, J., Zhou, X., Jiang, S., Tu, L., and Liu, X. (2020). Monsoon precipitation, economy and wars in ancient China. *Front. Earth Sci.* 8. doi: 10.3389/feart.2020.00317

Zhao, L., Ma, C., Zhang, X., Li, L., and Lu, H. (2024). Multi-proxy reconstruction of climate changes from the Medieval Climate Anomaly to the Little Ice Age in Southeast China. *Palaeogeogr. Palaeoclimatol. Palaeoecol.* 655, 112510. doi: 10.1016/j.palaeo.2024.112510

Zhao, B., Zhuang, G., and Cao, D. (1995). Circulation, tidal residual currents and their effects on the sedimentations in the Bohai Sea. *Oceanol. Limnol. Sin.* 26, 466–473.

Zhong, W., Wei, Z., Chen, Y., Shang, S., Xue, J., Ouyang, J., et al. (2017). A 15.4-ka paleoclimate record inferred from δ13C and δ15N of organic matter in sediments from the sub-alpine Daping Swamp, western Nanling Mountains, South China. *J. Paleolimnol.* 57, 127–139. doi: 10.1007/s10933-016-9935-x

Zhou, X., Jia, N., Cheng, W., Wang, Y., and Sun, L. (2013). Relocation of the Yellow River estuary in 1855 AD recorded in the sediment core from the northern Yellow Sea. *J. Ocean Univ. China* 12, 624–628. doi: 10.1007/s11802-013-2199-4

Zhou, X., Sun, L., Zhan, T., Huang, W., Zhou, X., Hao, Q., et al. (2016). Time-transgressive onset of the Holocene Optimum in the East Asian monsoon region. *Earth Planet. Sci. Lett.* 456, 39–46. doi: 10.1016/j.epsl.2016.09.052

Zhu, L., Cooper, D. J., Han, S., Yang, J., Zhang, Y., Li, Z., et al. (2021). Influence of the Atlantic Multidecadal Oscillation on drought in northern Daxing'an Mountains, Northeast China. *Catena* 198, 105017. doi: 10.1016/j.catena.2020.105017